



OPEN ACCESS

EDITED BY

Olaya Santiago Fernández,
Albert Einstein College of Medicine,
United States

REVIEWED BY

Yuyao Tian,
Massachusetts General Hospital and
Harvard Medical School, United States
Juan Antonio Fafian Labora,
University of A Coruña, Spain

*CORRESPONDENCE

Alejandro Ocampo,
✉ alejandro.ocampo@unil.ch

RECEIVED 17 October 2023

ACCEPTED 04 December 2023

PUBLISHED 23 January 2024

CITATION

Paine PT, Rechsteiner C, Morandini F,
Desdin-Micó G, Mrabti C, Parras A,
Haghani A, Brooke R, Horvath S,
Seluanov A, Gorbunova V and Ocampo A
(2024), Initiation phase cellular
reprogramming ameliorates DNA
damage in the ERCC1 mouse model of
premature aging.
Front. Aging 4:1323194.
doi: 10.3389/fragi.2023.1323194

COPYRIGHT

© 2024 Paine, Rechsteiner, Morandini,
Desdin-Micó, Mrabti, Parras, Haghani,
Brooke, Horvath, Seluanov, Gorbunova
and Ocampo. This is an open-access
article distributed under the terms of the
[Creative Commons Attribution License
\(CC BY\)](https://creativecommons.org/licenses/by/4.0/). The use, distribution or
reproduction in other forums is
permitted, provided the original author(s)
and the copyright owner(s) are credited
and that the original publication in this
journal is cited, in accordance with
accepted academic practice. No use,
distribution or reproduction is permitted
which does not comply with these terms.

Initiation phase cellular reprogramming ameliorates DNA damage in the ERCC1 mouse model of premature aging

Patrick Treat Paine^{1,2}, Cheyenne Rechsteiner³,
Francesco Morandini³, Gabriela Desdin-Micó¹, Calida Mrabti¹,
Alberto Parras^{1,4}, Amin Haghani⁵, Robert Brooke⁶,
Steve Horvath^{5,6,7}, Andrei Seluanov^{3,8}, Vera Gorbunova^{3,8} and
Alejandro Ocampo^{1,4*}

¹Department of Biomedical Sciences, Faculty of Biology and Medicine, University of Lausanne, Lausanne, Switzerland, ²Center for Virology and Vaccine Research, Harvard Medical School, Boston, MA, United States, ³Department of Biology, University of Rochester, Rochester, NY, United States, ⁴EPITERNA SA, Vaud, Switzerland, ⁵Altos Labs, San Diego, CA, United States, ⁶Epigenetic Clock Development Foundation, Torrance, CA, United States, ⁷Human Genetics, David Geffen School of Medicine, University of California, Los Angeles, Los Angeles, CA, United States, ⁸Department of Medicine, University of Rochester Medical Center, Rochester, NY, United States

Unlike aged somatic cells, which exhibit a decline in molecular fidelity and eventually reach a state of replicative senescence, pluripotent stem cells can indefinitely replenish themselves while retaining full homeostatic capacity. The conferment of beneficial-pluripotency related traits via *in vivo* partial cellular reprogramming in vivo partial reprogramming significantly extends lifespan and restores aging phenotypes in mouse models. Although the phases of cellular reprogramming are well characterized, details of the rejuvenation processes are poorly defined. To understand whether cellular reprogramming can ameliorate DNA damage, we created a reprogrammable accelerated aging mouse model with an ERCC1 mutation. Importantly, using enhanced partial reprogramming by combining small molecules with the Yamanaka factors, we observed potent reversion of DNA damage, significant upregulation of multiple DNA damage repair processes, and restoration of the epigenetic clock. In addition, we present evidence that pharmacological inhibition of ALK5 and ALK2 receptors in the TGF β pathway are able to phenocopy some benefits including epigenetic clock restoration suggesting a role in the mechanism of rejuvenation by partial reprogramming.

KEYWORDS

aging, DNA damage, ercc1, cellular reprogramming, TGF β

Introduction

The phenomenon of aging is directly linked to a decline in cellular repair functions with an associated increase in aging phenotypes including genomic instability (Rando and Chang, 2012; Kennedy et al., 2014; López-Otín et al., 2013). DNA damage events due to radiation, reactive oxygen species, chemicals, or replication errors can overwhelm DNA repair functions and are proposed as a causative factor for epigenetic dysregulation and a key contributor to age associated pathologies (Tubbs and Nussenzweig, 2017; Niedernh et al.,

2018; Kane and Sinclair, 2019; Schumacher et al., 2021; Yang et al., 2023). In this line, *Ercc1*^{Δ/-} progeroid mice, harboring a single truncated *Ercc1* allele required for nucleotide excision repair (NER), interstrand crosslink repair (ICL), and homologous repair display increased DNA damage and a broad spectrum of aging phenotypes including senescence, neurodegeneration, multimorbidity, and a shortened lifespan (Weeda et al., 1997; Dollé et al., 2006; de Waard et al., 2010; Vermeij et al., 2016; Li et al., 2019). Interestingly, a recent comparative lifespan analysis of 18 wildtype (WT) rodent species indicates DNA double-strand break repair was more efficient in long-lived species (Tian et al., 2019). For these reasons, DNA repair mutant *Ercc1*^{Δ/-} mice are an ideal alternative for investigating aging interventions and DNA repair-related mechanisms of rejuvenation in particular (Vermeij et al., 2016; Takayama et al., 2017; Birkisdóttir et al., 2021).

Cellular reprogramming can be defined as the conversion of a somatic cell to pluripotency and can be induced via the forced expression of four defined transcription factors; Oct4, Sox2, Klf4, and c-Myc (OSKM) (Takahashi and Yamanaka, 2006). The resulting induced pluripotent stem cells (iPSCs) exhibit a dedifferentiated cell identity similar to embryonic stem cells (ESCs) along with a restoration of aged phenotypes (Lapasset et al., 2011; Singh and Newman, 2018). Recently, *in vivo* partial reprogramming (IVPR), following short-term cyclic expression of OSKM, has emerged as a novel therapeutic strategy for the treatment of age-related diseases (ARDs) (Mahmoudi et al., 2019a; Alle et al., 2021; de Magalhães and Ocampo, 2022). Specifically, partial cellular reprogramming has produced improvements to lifespan, hallmarks of aging, the epigenetic clock, and tissue regeneration in progeroid and WT mouse models *in vivo* (Ocampo et al., 2016; de Lázaro et al., 2019; Lu et al., 2020; Sarkar et al., 2020; Chen et al., 2021; Wang et al., 2021; Alle et al., 2022; Browder et al., 2022; Cheng et al., 2022; Chondronasiou et al., 2022; Gill et al., 2022; Macip et al., 2023; Yang et al., 2023). Multiple *in vitro* time course studies have demonstrated reprogramming initially proceeds in a multifactorial manner involving extensive epigenetic remodeling, cell cycle induction with a shortened G1 phase, mesenchymal to epithelial transition due to TGFβ inhibition and BMP induction, while undergoing a major reset to the proteome and transcriptome (Maherali et al., 2007; Brambrink et al., 2008; Mikkelsen et al., 2008; Stadtfeld et al., 2008; Li et al., 2010; Samavarchi-Tehrani et al., 2010; Plath and Lowry, 2011; Buganim et al., 2012; Hansson et al., 2012; Polo et al., 2012; Benevento et al., 2014). Importantly, in what manner and to what extent these early alterations to molecular and cellular processes via IVPR counter and reverse aging drivers is currently unknown.

To address this limitation and gain a deeper understanding of the mechanisms involved in age amelioration by OSKM induction, we have chosen to investigate the effects of partial reprogramming in the *Ercc1*^{Δ/-} DNA damage model of accelerated aging. Using an *in vitro* time course capable of dissecting time dependent processes, we characterized the early events of reprogramming in a novel reprogrammable *Ercc1*^{Δ/-} accelerated aging mouse model. Most importantly, we observed a significant reduction in DNA damage beginning at 2 days of reprogramming demonstrating reversal of a key hallmark of aging. At the same time RNA seq analysis shows a significant upregulation of nearly every major DNA repair pathway while DNA methylation clock analysis shows a reversal of epigenetic

age. Interestingly, improvements were more robust in the *Ercc1* DNA damage model *versus* the WT cells, as would be expected from an improvement to homeostatic capacity. Lastly, small molecule inhibition of the TGFβ pathway was sufficient to phenocopy some rejuvenating aspects of reprogramming including a decrease in nuclear size, decreased γH2AX, and restoration of the epigenetic clock.

Results

Induced reprogramming in a mouse model of accelerated aging decreases DNA damage

OSKM-mediated partial cellular reprogramming has been shown to mitigate genomic instability and epigenetic alterations in WT and Lamin A mutant mouse fibroblasts as well as *in vitro* aged nucleus pulposus cells (Ocampo et al., 2016; Cheng et al., 2022). On other hand, it is currently unknown whether this restoration would occur in an *Ercc1* DNA damage model of accelerated aging with defects in DNA repair. To address this question, we developed a time course discovery platform utilizing a novel doxycycline-inducible mouse model of reprogrammable aging (*Ercc1*^{Δ/-} 4Fj^{+/-} rtTA^{+/-}) containing a single truncated *Ercc1* allele, Col1a1-tetO-OKSM polycistronic transgene, and the ROSA26-M2-rtTA allele (Figures 1A, B).

To first verify the presence of DNA damage in our reprogrammable progeria model, adult tail tip fibroblasts (FBs) were isolated from the 4Fj *Ercc1*^{Δ/-} (D/KO) and 4Fj *Ercc1*^{+/+} (WT) mice, stained for the DNA damage marker γH2AX, and imaged with confocal laser microscopy. As expected, a significant increase to γH2AX fluorescent intensity (artificial units) was observed in the D/KO fibroblasts compared to the WT (Figure 1C, Supplementary Figure S1A). In addition, this accelerated aging cell model also displayed a significant increase in nuclear area in these samples, based on nuclear staining with DAPI (Supplementary Figure S1B). This experiment confirmed the presence of a DNA repair defect in our novel OSKM inducible mouse model of aging along with an enlarged nucleus compared to WT (Supplementary Figures S1A, B).

In vitro cellular reprogramming time course experiments have previously been used to identify three phases of reprogramming including initiation, maturation, and stabilization (David and Polo, 2014; Kuno et al., 2018). Initiation phase proceeds via alterations to several key biological processes including proliferation, chromatin modification, DNA damage repair, mesenchymal to epithelial transition (MET), and RNA processing (Samavarchi-Tehrani et al., 2010; Koche et al., 2011; Buganim et al., 2012; Hansson et al., 2012; Polo et al., 2012; Benevento et al., 2014; Mahmoudi et al., 2019b; Gill et al., 2022; Roux et al., 2022). To gain insight into partial reprogramming processes with the capacity to restore homeostatic function in a DNA damage model, a time course analysis of the initiation phase of reprogramming was performed (Figure 1B). At the same time, the induction of pluripotency in somatic cells following OSKM expression is a stochastic, asynchronous, and inefficient process often taking weeks with a low percentage of iPSC colonies (Stadtfeld and Hochedlinger, 2010; Ebrahimi, 2015). To facilitate an accelerated reprogramming process and enhance the

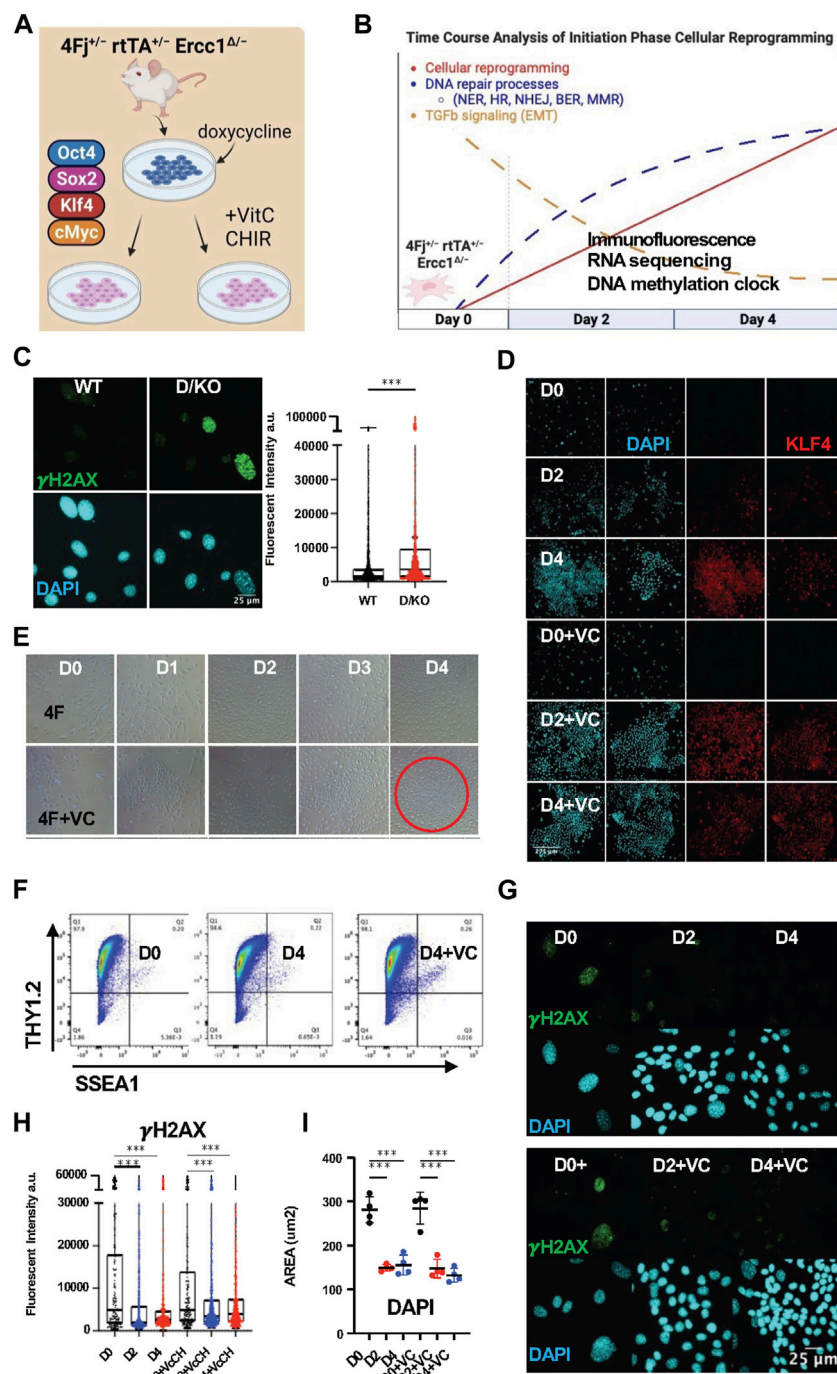


FIGURE 1

Initiation phase reprogramming in 4Fj ± rtTA ± Ercc1Δ/- accelerated aging model promotes DNA damage repair. (A) Illustration of doxycycline inducible cellular reprogramming Ercc1 mutant fibroblasts (Fb) alone or enhanced with small molecules. (B) Schematic of initiation phase timecourse analysis setup with observed changes to DNA repair and TGFb signaling. (C) Representative Immunofluorescence (IF) and quantification of γH2AX in fibroblasts from wildtype (WT) and Ercc1Δ/- (D/KO) mice, imaged with Nikon laser confocal spinning disc, according to Mann-Whitney test, *****p* < 0.0001. (D) IF of KLF4 and DAPI in 4Fj ± rtTA ± Ercc1Δ/- Fbs after 2 and 4 days doxycycline induction with or without VC at 100x (E) Time course analysis of 4F and 4F.D/KO Fb during 4 days of dox induction ± VC, brightfield (BF) images at 4x. (F) FACS analysis of reprogramming FBs at day 0 and day 4, stained with Thy1.2 and SSEA1. (G) IF of γH2AX and DAPI during time course analysis of 4F.D/KO Fb ± VC. (H) IF quantification of γH2AX levels during timecourse shows decrease levels at day 2 and day 4 according to one way ANOVA, *****p* < 0.001. (I) Quantification of DAPI area during timecourse shows decrease in size at day 2 and day 4 based on mean values of 4 experiments according to one way ANOVA, *****p* < 0.0001.

ability to delineate reprogramming-induced aging phenotypes in bulk cultures a previously identified small molecule combination, Vitamin C (V) and CHIR-99021 (C), was selected (Chen et al., 2011;

Bar-Nur et al., 2014; Vidal et al., 2014). Alone, Vitamin C is able lower the epigenetic barrier of pluripotent gene expression due to its function as a histone demethylase and Tet enzyme cofactor while

CHIR activates the Wnt pathway and promotes glycolysis via GSK3-beta inhibition (Li et al., 2009; Esteban et al., 2010; Liu et al., 2022).

To confirm the induction of cellular reprogramming following expression of OSKM in our reprogrammable DNA damage model, doxycycline (2ug/mL) was added to 4F Ercc1 cells in culture alone or combined with VC and imaged with brightfield microscopy at 4x during days 0–4 (Figures 1A, B). Expression of the Klf4 and Sox2 transcription factors were observed only after doxycycline induction with or without VC respectively but never day 0 based on immunofluorescence (IF) laser confocal imaging (Figure 1D, Supplementary Figure S1C). A clear shift in cell morphology with a cobblestone appearance associated with MET is present after 2 days, more so after 4 days, and most strongly in the enhanced D4+VC group (Figure 1E). Reprogrammed 4F WT fibroblasts exhibit the somatic identity marker Thy1.2 at D4 with or without VC, matching previous reports (Figure 1F). Together this data demonstrates initiation phase partial reprogramming is occurring *in vitro* in our 4F Ercc1 mouse model (Figure 1G, Supplementary Figure S1D).

In regards to the effects of cellular reprogramming on γ H2AX in this DNA damage model, we first used flow cytometry. Interestingly, 2 days of doxycycline induced reprogramming in the D/KO was sufficient to decrease median γ H2AX fluorescence (Supplementary Figure S1E). Next, using IF and confocal imaging, we observed a significant decrease in mean γ H2AX level per cell after 2 and 4 days of reprogramming (Figures 1G, H, Supplementary Figure S1J). Similarly, enhanced reprogramming with VC also restored this DNA damage marker significantly after 2 and 4 days of OSKM induction (Figures 1G, H, Supplementary Figure S1J). These D/KO cells also displayed a significant reduction in nuclear size during reprogramming after induction with doxycycline for 2 or 4 days (Figure 1I). When this experiment was repeated on OSKM inducible WT cells without the DNA repair defect, it also showed a significant decrease in γ H2AX signal and decrease in nuclear area (Supplementary Figure S1F). Thus, initiation phase cellular reprogramming is sufficient to ameliorate a key driver of aging even in mutant cells defective for DNA repair responsible for NER, ICL, and HR.

The DNA methylation clock is restored in Ercc1^{Δ/-} following short term reprogramming

Recent evidence from our lab indicates that D/KO FBs display accelerated aging based on the DNA methylation clock and are therefore a good *in vitro* model to investigate aging mechanisms and interventions (Perez et al., 2022). Furthermore, cellular reprogramming has been observed to reverse epigenetic age in mouse and human cell types but the effects on an accelerated aging model with a DNA repair defect are unknown (Horvath, 2013; Olova et al., 2019). In order to investigate the effect of reprogramming on the DNA methylation clock, we applied the DNA Methyl Age Skin Final clock to all samples and timepoints. Strikingly, enhanced reprogramming with VC for 4 days in the D/KO produced a significant restoration to the DNA methylation clock with the top responder showing a 54% decrease in epigenetic age (Figure 2A). At the same time, there was a trend towards epigenetic clock restoration after 2 and 4 days of reprogramming

although not significant, perhaps due to less efficient reprogramming (Figure 2A). Significant restoration to the DNAm clock only occurred at day 2 in WT FBs (Supplementary Figure S2A). In addition, variability was greater in the WT samples perhaps due to the stochastic nature of reprogramming and the early time point chosen for analysis, or the lack of accelerated aging phenotype (Supplementary Figure S2A). The robust reversal of the DNAm clock in the D/KO FBs indicates enhanced reprogramming is capable of cellular rejuvenation in an aging model with defective DNA repair.

Next, as chromatin remodeling and reversal of the DNA methylation clock are observed to coincide during cellular reprogramming, we sought to understand the epigenetic alterations that occur following reprogramming in this Ercc1 model (Koche et al., 2011; Olova et al., 2019). First, a significant increase in H3K9me3 was observed in the D/KO fibroblasts compared to WT controls based on IF confocal imaging at 100x (scale bar 25 um applies to all images) (Figure 2B, Supplementary Figure S2B). A similar increase was observed in the heterochromatin mark H4K20me3 while H3K27me3 remained unchanged under the same conditions (Supplementary Figures S2D,E). These results were then confirmed with western capillary analysis (Supplementary Figure S2C). We hypothesize that this *in vitro* phenotype of chromatin compaction is an adaptation in these cells to protect against chronic elevated DNA damage levels (Takata et al., 2013; Lee et al., 2020). Interestingly, when reprogramming or enhanced reprogramming was induced for 2 or 4 days, heterochromatin was significantly decreased in this DNA damage model shifting it towards WT levels (Figures 2C–E, Supplementary Figures S2F–I). This restoration of heterochromatin levels in D/KO FBs coincides with improvement to reversion of the DNAm clock, in line with previous reports suggesting a mechanistic relationship (Ocampo et al., 2016; Lu et al., 2020; Yang et al., 2023).

Homeostatic capacity is significantly upregulated during the initiation phase of cellular reprogramming

To better understand the effects of reprogramming in this DNA damage model, paired-end bulk RNA sequencing and analysis was performed for each treatment and time point. Principal component analysis (PCA) based on relative gene expression values confirmed groups clustered based on the treatment, timepoint, and cell type while displaying a reprogramming trajectory from day 0 to day 4 (Figure 3A). Interestingly, the enhanced reprogramming at day 2 plus VC was equal to 4 days of reprogramming alone based on overlapping PCA scores (Figure 3A). At the same time, D/KO cells displayed a larger shift in PC2 score than WT following reprogramming (Figure 3A). Venn diagrams and associated gene expression heat maps were created based on the normalized transcriptomes from each group and demonstrate a shared gene profile during reprogramming albeit with some unique differences (Figures 3B, C). In particular, over 1,400 genes were uniquely upregulated and 992 downregulated in the D/KO FBs during initiation phase with enhanced reprogramming compared to reprogrammed WT cells (Figure 3C). The most robust changes

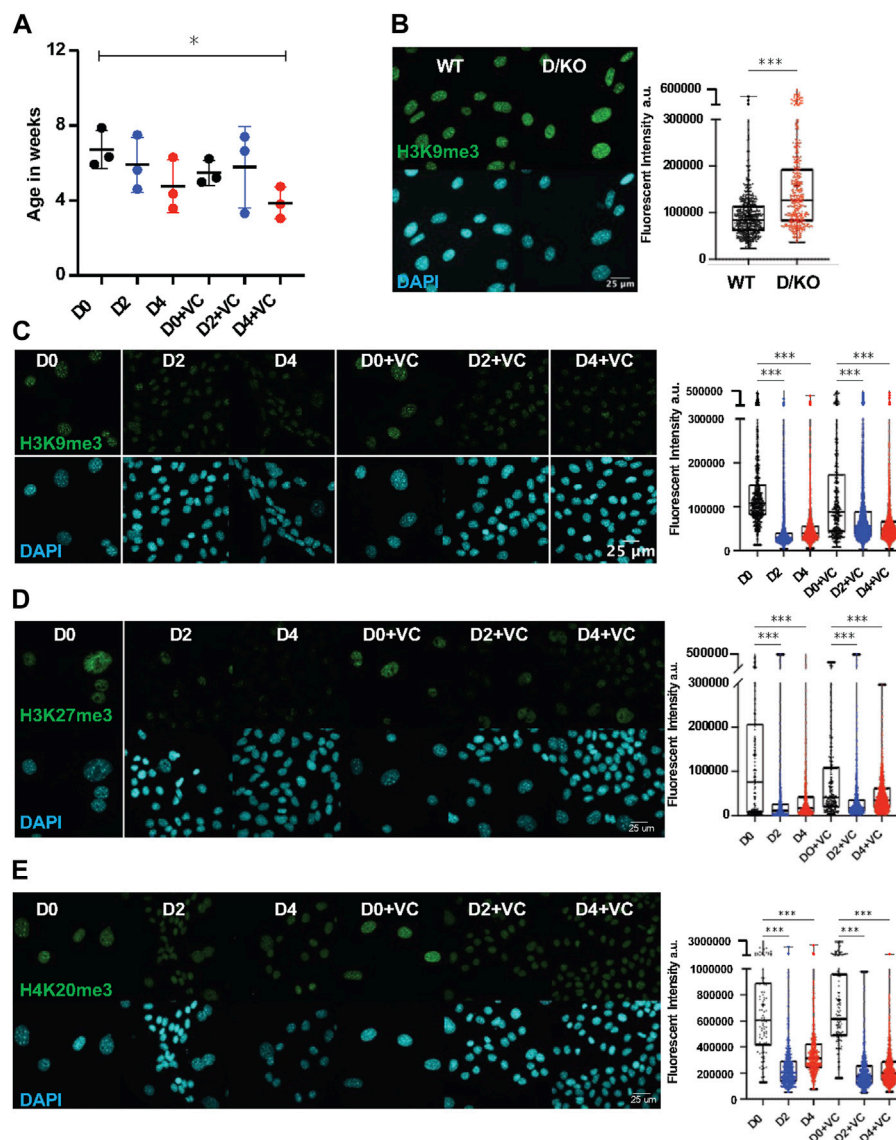


FIGURE 2

DNA methylation clock is restored in *Ercc1Δ/−* following short term reprogramming. **(A)** DNA methylation clock (DNA Methylation Age Skin Final clock) analysis of cellular *Ercc1* mutant Fb during time course, $n = 3$, $*p < 0.05$ according to unpaired t -test. **(B)** IF and quantification of H3K9me3 in fibroblasts from WT and D/KO mice, imaged with Nikon laser confocal spinning disc, according to Mann-Whitney test, $***p < 0.0001$. **(C)** IF and quantification of H3K9me3 and DAPI during time course in 4F.D/KO Fbs after 2 and 4 days doxycycline induction with or without VC at 100x according to Kruskal–Wallis test, $*p < 0.0001$ **(D)** IF and quantification of H3K27me3 and DAPI during time course in 4F.D/KO Fbs after 2 and 4 days doxycycline induction with or without VC at 100x according to Kruskal–Wallis test, $*p < 0.0001$ **(E)** IF and quantification of H4K20me3 and DAPI during time course in 4F.D/KO Fbs after 2 and 4 days doxycycline induction with or without VC at 100x according to Kruskal–Wallis test, $*p < 0.0001$.

were observed following enhanced reprogramming to the D/KO group, indicating a profound and rapid reset to the transcriptome in this DNA damage model (Figures 3B, C). GO term analysis demonstrated a significant upregulation of DNA damage repair pathways in the D/KO enhanced reprogramming group including DNA repair, homologous recombination (HR), non-homologous end joining (NHEJ), base excision repair (BER), mismatch repair (MMR), nucleotide excision repair (NER), and alternative end joining (AltEJ), while interstrand crosslink repair (ICR) showed a trend towards upregulation. (Figure 3D, S3a). At the same time, reprogramming in WT cells did not produce such broad and robust effects on DNA repair processes (Figure 3D, Supplementary Figure S3A). Other

notable processes increased with enhanced reprogramming include chromatin organization pathways in D/KO cells (Figure 3D, Supplementary Figure S3A). Importantly, there was also a significant downregulation in TGF β receptor signaling and TGF β regulation pathways as well as a decrease in EMT pathways (Figure 3D, Supplementary Figure S3A). Gene set enrichment analysis (GSEA) showed that intermediate filament cytoskeleton organization and processes, keratinocyte differentiation and epidermal differentiation were significantly upregulated at all timepoints and models (Supplementary Figure S3B). At the same time, Reactome analysis showed that Keratinization and Formation of the Cornified Envelope were also universally upregulated

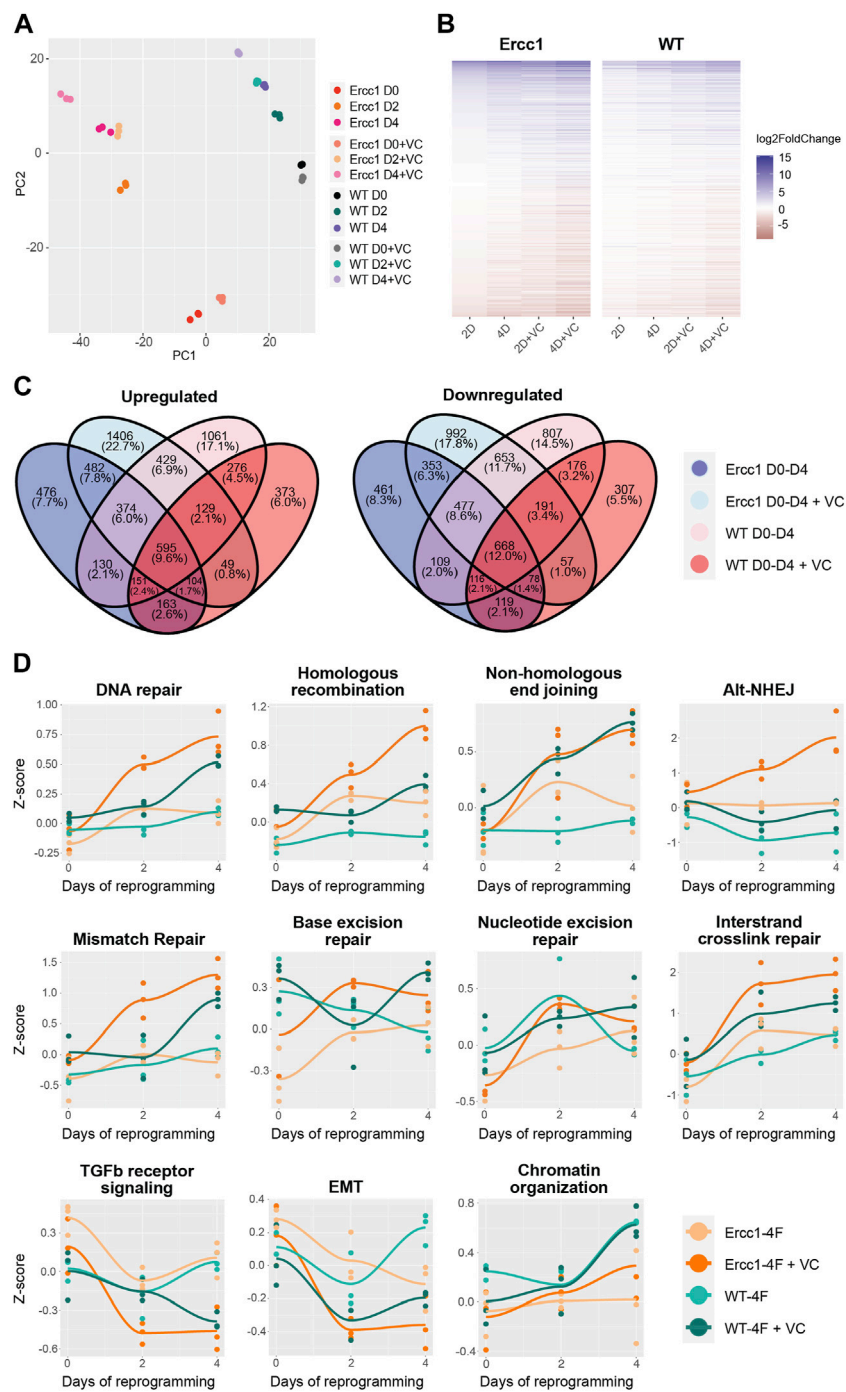


FIGURE 3

Initiation phase reprogramming drives transcriptomic reset and upregulates DNA repair and chromatin organization in *Ercc1* Δ/Δ . **(A)** Principal component analysis (PCA) of the *Ercc1* and WT reprogramming at days 0, 2, and 4 with and without VC enhancement. Principal components 1 and 2 are shown. **(B)** Heat map comparing *Ercc1* and WT reprogramming at all timepoints, models, and treatments. Genes with a *p*-value lower than $1e-18$ in at least one condition are shown. **(C)** Venn Diagram showing the overlap of significant DEGs (adjusted *p*-value < 0.05) in *Ercc1* and WT during IP reprogramming with and without VC enhancement. Genes were evaluated using a continuous model over 4 days of reprogramming. **(D)** Reprogramming trajectory visualizations based on median Z-scores of genes from significantly up or downregulated GO pathway including DNA repair, TGFb signaling, EMT, and chromatin organization ($n = 3$).

(Supplementary Figure S3C). Together, this transcriptomic data provides a mechanistic basis that supports the observed changes to morphological, epigenetic, and DNA damage phenotypes that occur following short-term reprogramming in our DNA damage model.

Interestingly, the robust upregulation of major DNA repair processes in the *Ercc1* model vs. WT suggest a homeostatic process capable of responding to intrinsic molecular and age-related defects that characterized *Ercc1* cells.

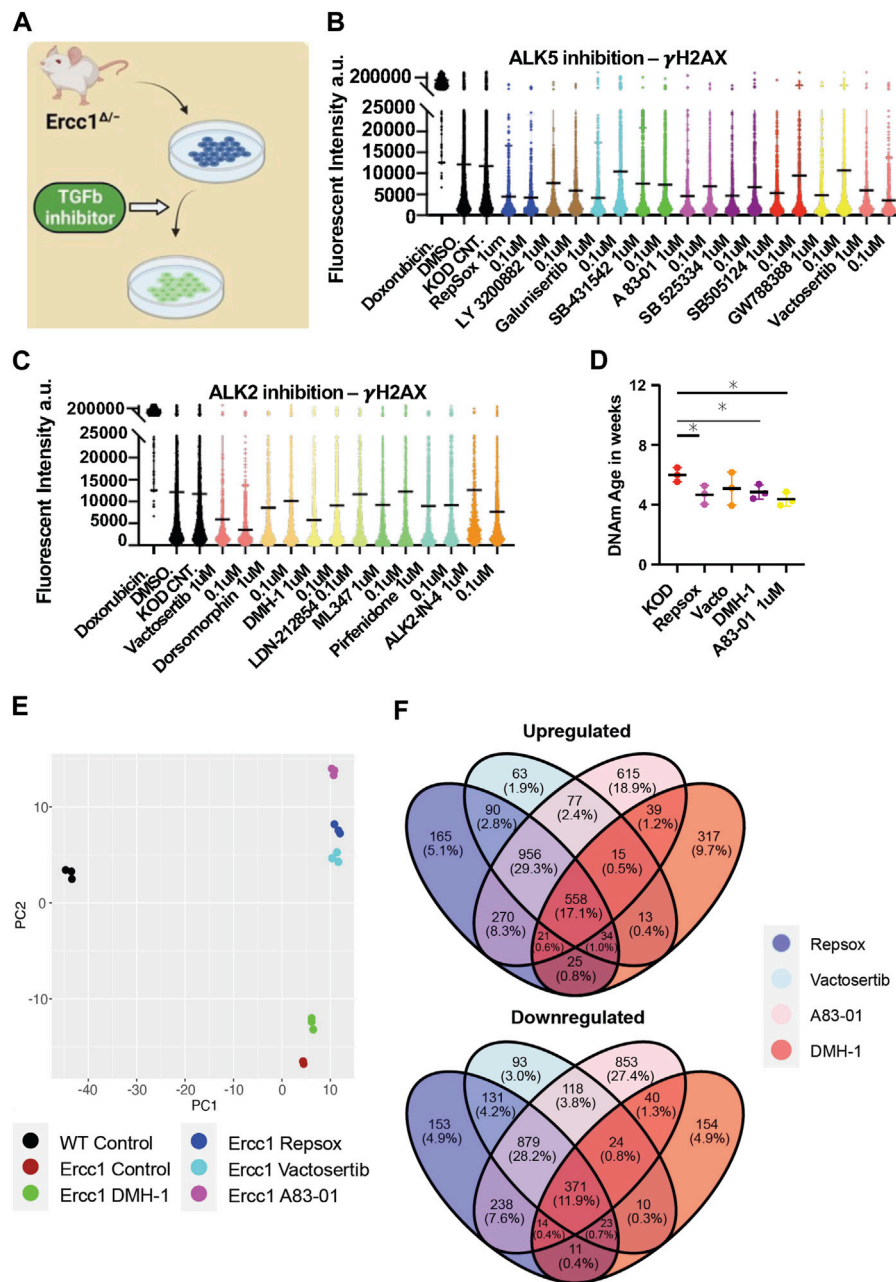


FIGURE 4

Inhibition of ALK5 or ALK2 receptors improves DNA damage phenotype and resets the DNA methylation clock and transcriptome in *Ercc1Δ/−*. **(A)** Illustration of TGFB inhibitor screen on D/KO Fbs. **(B)** IF quantification of γ H2AX mean levels in D/KO Fbs following treatment with ALK5 inhibitors, plated in 96 wells in triplicate and imaged with laser confocal at 40x. **(C)** IF quantification of γ H2AX mean levels in D/KO Fbs following treatment with ALK2 inhibitors, plated in 96 wells in triplicate. **(D)** DNA methylation clock (DNA Methylation Age Skin Final clock) analysis, comparing Repsox (0.1 μ m), Vactosertib (0.1 μ m), DMH-1 (1.0 μ m), and A83-01 (1.0 μ m) on D/KO Fbs, $n = 3$, $*p < 0.05$ according to unpaired t -test. **(E)** Principal component analysis (PCA) of *Ercc1* cells treated with TGFB inhibitors. Principal components 1 and 2 are shown. **(F)** Venn Diagram showing the overlap of significant genes (adjusted p -value < 0.05) for the TGFB inhibitors.

TGFB inhibition alone improves DNA damage phenotypes and rejuvenates the DNA methylation clock

The RNA seq analysis showing downregulation of TGFB signaling and associated epithelial to mesenchymal transition pathways is a well-documented early event of cellular reprogramming following OSKM induction (Maherali et al., 2007; Li et al., 2010; Samavarchi-Tehrani

et al., 2010; Mah et al., 2011). In contrast, upregulation of TGFB signaling is a driver of aging phenotypes including cell degeneration, fibrosis, ROS, inflammation, DNA damage, senescence, and stem cell aging (Lyu et al., 2018; Tominaga and Suzuki, 2019; Kim et al., 2021; Liu et al., 2021). Recently our lab observed that inhibition of the TGFB pathway is able to extend lifespan in *C. elegans*, supporting its role in aging and longevity (Schoenfeldt et al., 2022). Based on these observations, we asked whether TGFB inhibition alone could impact DNA damage and the DNA

methylation clock in our *Erccl* accelerated aging model in a manner similar to reprogramming (Figure 4A). The TGF β superfamily consists of over 30 subtypes but for this study we focused on canonical TGF β signaling and the bone morphogenic protein pathway (BMP). Both are important for early stage reprogramming as inhibition of TGF β or expression of BMP are important drivers of the MET (Samavarchi-Tehrani et al., 2010; Weiss and Attisano, 2013; Bar-Nur et al., 2014). Specifically, 9 inhibitors that target the TGF β ALK5 receptor and 6 inhibitors that target the BMP ALK2 receptors were screened for 3 days on D/KO fibroblasts. Following a cell viability study to confirm a safe dosage range, a high or low dose of each inhibitor was added to the *Erccl* fibroblasts for 3 days and analyzed for changes to γ H2AX using IF and confocal microscopy (Supplementary Figure S4A). All of the ALK5 inhibitors successfully decreased γ H2AX levels based on IF, although in some cases it was dose-dependent (Figure 4B). Interestingly, all but one of the ALK2 inhibitors also decreased DNA damage in *Erccl* fibroblasts, although not as effectively as the ALK5 inhibitors, again in a dose dependent manner (Figure 4C). Subsequently, we repeated these experiments with only the top performers including ALK5 inhibitors Repsox and A83-01, ALK2 inhibitor DMH-1, and dual ALK5 and ALK2 inhibitor Vactosertib. Once again, each of the inhibitors decreased the γ H2AX signal of *Erccl* fibroblasts below control levels although the ALK2 inhibitor, DMH-1, was less effective than the three ALK5 inhibitors (Supplementary Figure S4B). Subsequently, when nuclear area was calculated based on DAPI staining, DMH-1 was also the only inhibitor not to show a trend towards decreased nuclear size potentially suggesting an association between nuclear size changes and improvements in DNA repair (Supplementary Figure S4). In contrast, other small molecules previously shown to induce pluripotency when applied as a cocktail were unable to decrease γ H2AX levels in *Erccl* fibroblasts when applied individually including valproic acid (VPA), CHIR, tranilcypromine (TCP), Forskolin, DZNep, or TTNPB (Supplementary Figure S4C) (Hou et al., 2013; Guan et al., 2022). When the ALK5 inhibitor, Repsox, was combined with 4 days of reprogramming, no added benefit to γ H2AX levels was observed (Supplementary Figure S4D). Finally, significant rejuvenation of the DNA methylation clock was observed with 3 of the 4 inhibitors, including Repsox, A83-01, and DMH-1 (Figure 4D). This data demonstrates that ALK5 and ALK2 inhibition is able to reduce DNA damage and restore the DNA methylation clock in this *Erccl* accelerated aging model.

RNA-seq analysis was next performed in *Erccl* FBs following treatment with these four TGF β inhibitors to better understand the mechanistic basis for improved DNA damage and a rejuvenated DNA methylation clock with ALK2 or ALK5 inhibition. Notably, PCA scores show the three ALK5 inhibitors cluster tightly together compared to the ALK2 inhibitor (Figure 4E). Interestingly, all 4 inhibitors shifted the D/KO transcriptome along the PC2 axis in the direction of WT cells with the greatest change observed following treatment with A83-01 (Figure 4E). At the same time, Venn diagrams show 558 genes were upregulated and 371 downregulated by all 4 inhibitors indicating similarity in gene expression profile regardless of target receptor (Figure 4F). Next, gene set enrichment analysis (GSEA) shows significant decreases to spindle checkpoint signaling with Repsox, Vactosertib, and A83-01 but not with DMH-1 (Supplementary Figure S4E). DMH-1 had a unique effect on upregulation of response to virus, response to interferon-gamma, and response to interferon-beta among

others based on the GSEA (Supplementary Figure S4E). Repsox uniquely induced upregulation to developmental-related gene sets including embryonic hindlimb morphogenesis, hindlimb morphogenesis, and midbrain development (Supplementary Figure S4E). Reactome analysis showed that DMH-1 also uniquely increased interferon signalling (Supplementary Figure S4E). Interestingly, GO term analysis demonstrated that all four inhibitors significantly downregulated several biological processes including mitotic cell cycle and canonical glycolysis (Supplementary Figure S5A). In line with previous publications showing TGF β inhibition disrupts DNA repair processes in cancer cells and HSCs, these four inhibitors also disrupted several DNA repair processes in our *Erccl* FBs (Supplementary Figure S5A) (Zhang et al., 2016; Pal et al., 2017; Liu et al., 2019; Liu et al., 2021). Interesting exceptions include a significant improvement to NER by DMH-1 and a trend towards upregulated ICL repair amongst all (Supplementary Figure S5A). Together this data shows ALK5 and ALK2 inhibitors are capable of decreasing the DNA damage marker γ H2AX and restoring the DNA methylation clock in *Erccl* fibroblasts while sharing some changes to the transcriptomic profiles.

TGF β inhibition phenocopies aspects of initiations phase cellular reprogramming

To investigate and compare shared rejuvenation processes between cellular reprogramming and TGF β inhibition, we next evaluated significant transcriptomic changes among the different treatments. Notably, a heatmap of significantly up or downregulated genes among the different treatments indicate a similar profile (Figure 5C). Specifically, 684 shared DEGs were upregulated and 627 downregulated following treatment with the ALK5 inhibitors Repsox, A83-01, Vactosertib, and reprogramming at day 4 (Figure 5A). Notably, gene expression changes induced by the 4 inhibitors shared a positive correlation with gene expression changes induced by reprogramming (Figure 5B). The strongest correlation was observed between the three ALK5 inhibitors and D4 reprogramming (Figure 5B, Supplementary Figure S5B). Interestingly, A83-01 was the closest in transcriptomic profile to day 4 reprogramming while Repsox was the closest to D4 enhanced reprogramming (Figure 5B, Supplementary Figure S5B). The top GO terms that were significantly downregulated with either reprogramming or the TGF β inhibitors include external encapsulating structure organization, extracellular matrix organization, extracellular structure organization, collagen fibril organization, skeletal system development and protein hydroxylation (Figure 5D). The most significantly upregulated GO terms shared by both D4 reprogramming and TGF β inhibition include steroid biosynthetic process, regulation of steroid biosynthetic process, alcohol biosynthetic process, organic hydroxyl compound metabolic process, epidermal cell differentiation, and alcohol metabolic process (Figure 5D). Reactome analysis of shared processes between reprogramming and Repsox, A83-01, and Vactosertib showed upregulation of complement cascade and downregulation of collagen formation and ECM organization (Figure 5E).

Interestingly, significant differences were noted when comparing the transcriptomic effects of reprogramming vs. TGF β inhibition on DNA repair processes even though both improved the DNA damage phenotype. Specifically, TGF β inhibition significantly downregulated multiple DNA repair processes in *Erccl* fibroblasts including AltEJ, NHEJ, and HR among others while reprogramming significantly

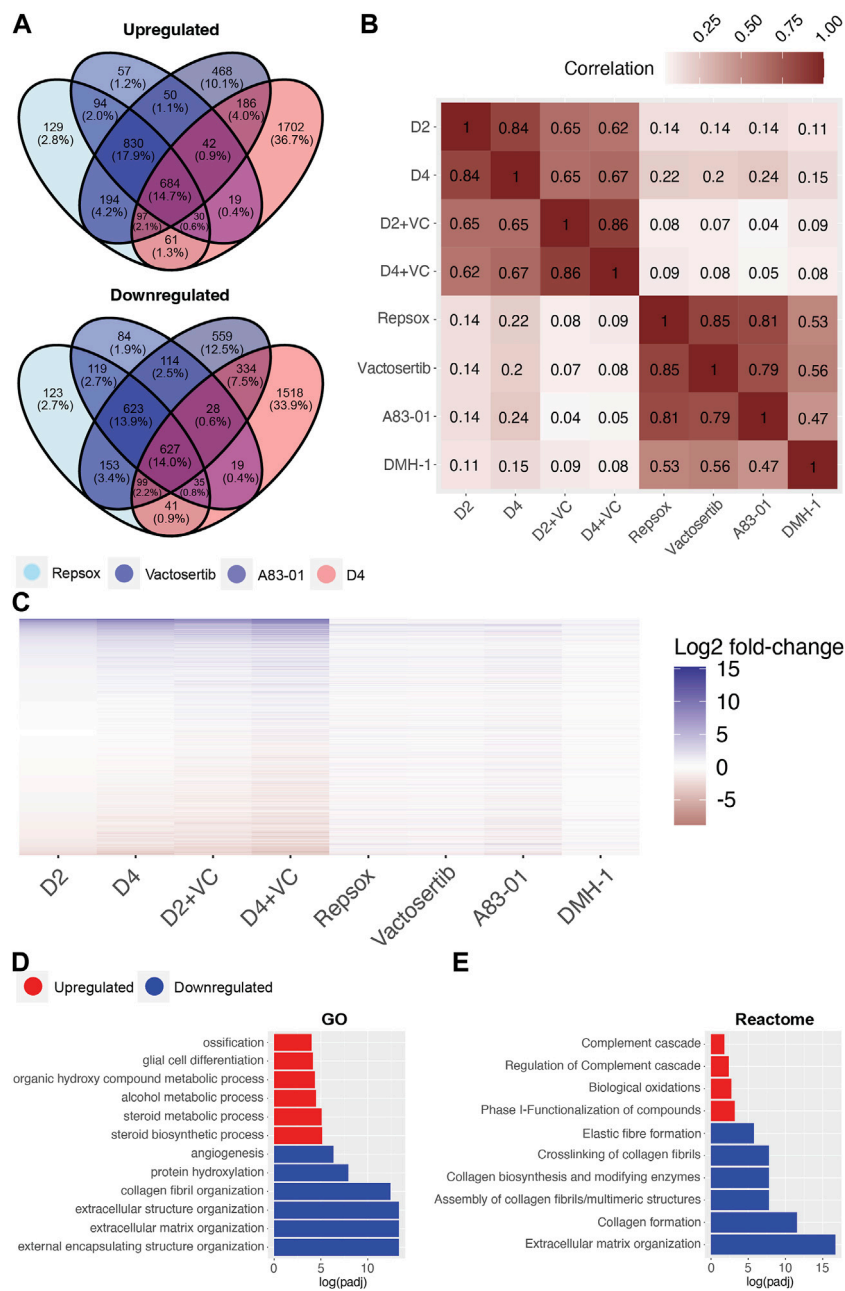


FIGURE 5

Transcriptomic comparison of Initiation phase reprogramming with TGFb inhibition in *Ercc1Δ/−*. **(A)** Venn Diagram showing the overlap of significant genes (adjusted *p*-value < 0.05) for ALK5 inhibitors and 4 days of reprogramming. **(B)** Pairwise correlation between the log2 fold-changes of the filtered gene set (*n* = 16,883) of *Ercc1* reprogramming and ALK5 or ALK2 inhibitors. **(C)** Heat map comparing *Ercc1* reprogramming with TGFb inhibitors. Genes with a *p*-value lower than 1e-10 in at least one condition are shown. **(D,E)** GO and Reactome analysis of the intersect of significant genes as evaluated in 5A. Terms with the top six upregulated (red) and downregulated (blue) assessed by log (adjusted *p*-value) are shown.

upregulated them (Supplementary Figure S5A, Supplementary Figure S3B). At the same time, only DMH-1 matched reprogramming by significantly upregulating NER, while Repsox and Vactosertib showed a trend towards improvement (Supplementary Figure S5A). In sum, this transcriptomic data demonstrates that TGFb inhibition and initiation phase reprogramming share a strong correlation in changes to gene expression. At the same time, reprogramming induces a more robust effect, especially on DNA repair processes in our reprogrammable *Ercc1* aging model.

Discussion

Although the age ameliorating effects of *in vivo* partial reprogramming have been well documented, the mechanistic drivers of rejuvenation by reprogramming are currently lacking (Singh and Newman, 2018). Interestingly, the robust alterations to biological processes that occurs during the initiation phase of cellular reprogramming including proliferation, chromatin modification, DNA damage repair, MET, and RNA processing are well

characterized and could potentially represent mechanistic drivers of longevity (Samavarchi-Tehrani et al., 2010; Koche et al., 2011; Buganim et al., 2012; Hansson et al., 2012; Polo et al., 2012; Benevento et al., 2014). For these reasons, we investigated the relationship between these early reprogramming induced changes and their impact on aging phenotypes. Specifically, we developed a reprogrammable DNA damage model of accelerated aging, *Ercc1^{Δ/-} 4Fj^{+/-} rtTA^{+/-}*, in order to test the impact of initiation phase reprogramming on a key driver of aging, genomic instability. As OSKM inhibits TGFβ signaling and drives the MET during initiation phase reprogramming, we investigated the mechanistic basis of rejuvenation via cellular reprogramming by comparing it to TGFβ inhibition (David and Polo, 2014). Due to the slow, stochastic, and asynchronous reprogramming process which confounds molecular studies in bulk cultures we also utilized a previously defined enhanced method of cellular reprogramming by adding ascorbic acid and CHIR-99021 to the culture media (Li et al., 2009; Bar-Nur et al., 2014; Liu et al., 2022).

Here we observed that OSKM expressing *Ercc1* cells undergo robust reprogramming induced changes to morphology, nuclear size, epigenome, transcriptome, and homeostasis related DNA repair processes. Striking improvements to the DNA damage marker γH2AX in our *Ercc1* fibroblasts with a defective repair process occurred within 2 days of pluripotency factor expression. At the same time, the elevated heterochromatin markers H3K9me3 and H4K20me3 were significantly restored following enhanced reprogramming for 2 and 4 days. Most notably, DNA methylation clock analysis shows significant rejuvenation in these *Ercc1* cells after 4 days of enhanced reprogramming. RNA sequencing analysis of the transcriptome showed several GO processes were upregulated significantly including DNA repair, chromatin organization, and mitotic cell cycle. This is consistent with pluripotency transcription factors being upstream of DNA repair mechanisms, particularly those acting on DNA double-strand breaks marked by γH2AX (Lu et al., 2022). Simultaneously, TGFβ signaling and EMT processes were significantly downregulated.

As TGFβ signaling is a driver of many aging phenotypes, we further investigated the importance of this signaling pathway to reprogramming induced rejuvenation via inhibition of the TGFβ receptor ALK5 or the BMP receptor ALK2 (Weiss and Attisano, 2013; Tominaga and Suzuki, 2019). Interestingly, nearly every TGFβ inhibitor tested significantly decreased γH2AX levels in *Ercc1* fibroblasts. The ALK5 inhibitors showed a more robust impact than ALK2 inhibitors on γH2AX levels while also decreasing nuclear size, a common phenotype observed during reprogramming. The lack of effect on nuclear size by ALK2 inhibition is in line with previous reports that show BMP signaling plays a role in driving MET during reprogramming (Samavarchi-Tehrani et al., 2010). Importantly improvement of the epigenetic clock was observed following treatment with 3 of 4 TGFβ inhibitors able with a distinct transcriptomic profile for the ALK5 and ALK2 inhibitors. Further analysis showed a strong correlation between TGFβ inhibition and cellular reprogramming based on similar changes to hundreds of DEGs. Interestingly, the robust changes to DNA repair based on GO pathway analysis was unique to OSKM expression. Previous work has shown that activation of the TFGb pathway promotes genomic instability and induces HR defects while inhibition reduces DNA damage, senescence, and aging phenotypes (Kanamoto et al., 2002; Liu et al., 2014; Pal et al., 2017; Tominaga and Suzuki, 2019). Interestingly, TGFβ inhibition has a disruptive effect on many DNA repair processes while selectively

promoting others in a cell type specific manner similar to our observations (Zhang et al., 2016; Liu et al., 2021).

Although initiation phase reprogramming in WT and *Ercc1* fibroblasts was capable of ameliorating the DNA damage marker γH2AX, the scale of effect was far more robust in the DNA damage model as demonstrated by significant increases in all major DNA repair processes. This data suggests that cellular reprogramming is sensitive to intrinsic cell state cues and drives a restoration of homeostatic function and youthful molecular phenotypes. Similarly, *in vivo* partial reprogramming studies show a more robust improvement to lifespan in progeria models indicating an ability to respond to deleterious cell states (Ocampo et al., 2016; Alle et al., 2022). Previously, it was shown improved DNA repair via overexpression of the HR protein Rad51 enhances reprogramming efficiency (Lee et al., 2016). In our 4F *Ercc1* fibroblasts, we observed the most significant reprogramming-induced rejuvenation coincided with upregulation of multiple DNA repair pathways. Recently maturation phase transient reprogramming for 13 days was shown to reverse the epigenetic clock in aged donors by up to 30 years but longer periods saw diminished benefits (Gill et al., 2022). Other groups have shown a single short burst of reprogramming *in vivo* is sufficient to ameliorate aging hallmarks and tissue-specific physiology (Alle et al., 2022). The precise mechanism of rejuvenation involved is unknown although several studies, including ours, supports a mechanistic contribution from the epigenetic remodeling process (Manukyan and Singh, 2014; López-León et al., 2017; Kane and Sinclair, 2019; Lu et al., 2020; Yang et al., 2023). Importantly, by inducing initiation phase reprogramming in an *Ercc1* model with an accelerated epigenetic clock, we observed early reprogramming coincided with TGFβ inhibition, improved homeostasis, DNA repair, and epigenetic rejuvenation. Notably, attempts to replicate OSKM-induced TGFβ inhibition with small molecule inhibitors phenocopied improvements to the epigenetic clock in this *Ercc1* model while decreasing the DNA damage marker γH2AX. Transcriptomic comparisons between cellular reprogramming and TGFβ inhibitors of the ALK5 and ALK2 receptors were positively correlated and shared similar changes to hundreds of DEGs. At the same time, the robust upregulation of DNA repair processes via initiation phase reprogramming compared to TGFβ inhibition alone suggests a different mechanistic route to DNA damage repair.

In conclusion, delineating the specific basis of rejuvenation remains difficult and potentially confounded by the multifactorial sequence of events necessary for reprogramming to proceed. The data here supports the premise that TGFβ inhibition is a mechanistic contributor to rejuvenation induced by cellular reprogramming. This work sets the stage for further mechanistic investigations into the early events of reprogramming to better understand the associated drivers of rejuvenated phenotypes.

Methods

Animal housing

These experiments were performed in accordance with Swiss legislation and after approval from the local authorities (Cantonal veterinary office, Canton de Vaud, Switzerland). Mice were housed in groups of five per cage or less with a 12h light/dark cycle between 06:00 and 18:00 in a temperature-controlled environment at 25°C and

humidity between 40% and 70%, with access to water and food. Wild type, premature aging, and programmable mouse models generated were housed together in the Animal Facilities of Epalinges and Department of Biomedical Science of the University of Lausanne.

Mouse strains

Ercc1^{Δ/-} mice and littermate controls *Ercc1*^{+/+} were generated in a C57BL6J|FVB hybrid background as previously generated and described by [de Waard et al. \(2010\)](#). Reprogrammable 4Fj^{+/-} rtTA^{+/-} *Ercc1*^{Δ/-} (4F.D/KO) and 4Fj^{+/-} rtTA^{+/-} *Ercc1*^{+/+} (4F.WT) mice strains were generated in a C57BL6J|FVB hybrid background following crosses with the previously described 4Fj mouse developed by [Carey et al. \(2010\)](#). Previously described wildtype reprogrammable cells with an Oct4-EGFP reporter were derived from mice carrying a polycistronic cassette containing Oct4, Sox2, Klf4, c-Myc, and a single allele EGFP in the *Col1a1* locus (OKSM) ([Stadtfeld et al., 2010](#)).

Mouse monitoring and euthanasia

All mice were monitored three times per week for their activity, posture, alertness, body weight, presence of tumors or wound, and surface temperature. Males and females were euthanized at by CO₂ inhalation (6 min, flow rate 20% volume/min). Subsequently, tail tip fibroblasts were harvested and cultured.

Cell culture and maintenance

Tail tip fibroblasts (TTF) were extracted from mice using Collagenase I (Sigma, C0130) and Dispase II (Sigma, D4693) and cultured in DMEM (Gibco, 11960085) containing 1% non-essential amino acids (Gibco, 11140035), 1% GlutaMax (Gibco, 35050061), 1% Sodium Pyruvate (Gibco, 11360039) and 10% fetal bovine serum (FBS, Hyclone, SH30088.03) at 37°C in hypoxic conditions (3% O₂). Subsequently, fibroblasts were cultured and passaged (3 or less) according to standard protocols. Reprogrammable TTF cells used in experiments were from young mice, including 4Fj^{+/-} rtTA^{+/-} *Ercc1*^{Δ/-} and 4Fj^{+/-} rtTA^{+/-} *Ercc1*^{+/+} (8 week old male), and 4Fj^{+/-} OCT4-GFP TTF (22 week old female). Non-reprogramming *Ercc1* TTF used include *Ercc1*^{Δ/-} and *Ercc1*^{+/+} (8 week old male) TGFb inhibitors were applied for 3 days, relevant to 2 or 4 days of reprogramming, and used *Ercc1*^{Δ/-} cells (4 week old female) and *Ercc1*^{+/+} TTF cells (14 week old female). Induction of the OSKM reprogramming factors *in vitro* followed treatment with doxycycline 2ug/mL in culture media for the specified time points. Enhanced reprogramming followed the same protocols but added fresh ascorbic acid (50ug/mL) and CHIR-99201 (3uM) as previously reported ([Bar-Nur et al., 2014](#)).

Immunofluorescence staining

Following experiments in 96 well plates or 24 well plates, TTF were washed with fresh PBS and fixed with 4% paraformaldehyde (Roth, 0964.1) in PBS at room temperature (RT) for 15 min. Then cells were washed 3 more times, followed by blocking and permeabilization step in

1% bovine serum albumin (Sigma, A9647-50G) in PBST (0.2% Triton X-100 in PBS) for 1 h (Roth, 3051.3). TTF were then incubated at 4°C overnight with a primary antibody, washed in PBS, followed by incubation with a secondary antibody and DAPI staining at room temp. for 1 h. If performed in 24 well plates, coverslips were used and mounted with Fluoromount-G (ThermoFisher, 00-4958-02), dried at RT in the dark, and stored at 4°C until ready to image or -20°C for long-term.

Immunofluorescence imaging

Confocal image acquisition was performed using the NIKON Ti2 Yokogawa CSU-W1 Spinning Disk, using the ×100 objective and with 15 z-sections of 0.3 μm intervals. Lasers for each antibody were selected (405 nm and 488 nm) with a typical laser intensity set. Exposure time and binning were established separately to assure avoidance of signal saturation.

Antibodies and compounds

Antibodies include: Abcam: anti-H3K27me3 (ab192985); Cell Signaling: anti-H3K9me3 (13,969), anti-H4K20me3, anti-γH2AX (9718); Roth: DAPI (6843.1) Compounds include: Cayman; Valproic Acid (13,033), CHIR99021 (13,122), Repsox (14,794), Forskolin (11,018), Doxorubicin (15,007); Acros Organics: TCP (130472500); APEXBIO: DZNep (A8182); Selleckchem: TTNPCP (S4627); Roth: X-beta-Gal (2315.3), Ascorbic Acid (Sigma).

Flow cytometry

Cells were stained with Thy1.2-APC and SSEA1-PE (Biolegend). Cells were fixed in BD Fixation and Permeabilization Solution. A Bectman Coulter Cytoflex S flow cytometer determined cellular subpopulation ratios.

RNA sequencing, processing, analysis

Total RNA and DNA was extracted from the same samples. Total RNA was extracted from cell samples in triplicate using the Qiagen AllPrep DNA/RNA Micro Kit (New England Biolab) and protocols were followed. Total RNA concentrations were determined using the Qubit RNA BR Assay Kit (ThermoFisher, Q10211).

The RNA-Seq library preparation and sequencing was done by Novogene (United Kingdom) Company Limited on an Illumina NovaSeq 6000 in 150 bp paired-end mode. Raw FASTQ files were evaluated for quality, adapter content and duplication rates with FastQC. Reads were trimmed using TrimGalore (https://www.bioinformatics.babraham.ac.uk/projects/trim_galore/) and aligned to the GRCm39 mouse genome assembly using Hisat2 (<https://doi.org/10.1038/s41587-019-0201-4>). Number of reads per gene were measured using the featureCounts function in the subread package ([Liao et al., 2013](#)).

All subsequent analysis was performed in R. DESeq2 was used to normalize raw read counts and perform differential gene expression analysis (doi:10.1186/s13059-014-0550-8). Ensembl gene IDs were mapped to gene symbols via the mapIds function in the

AnnotationDbi package (Pagès H, Carlson M, Falcon S, Li N (2023). *AnnotationDbi: Manipulation of SQLite-based annotations in Bioconductor*) with an org.Mm.e.g.,db reference package (Carlson M (2019). *Org.Mm.e.g.,db: Genome wide annotation for Mouse*). The clusterProfiler package (doi:10.1089/omi.2011.0118, doi:10.1016/j.xinn.2021.100141) was used to perform gene set enrichment analysis (GSEA) on gene ontology and Reactome terms.

DNA extractions

Total DNA was extracted from cells, in triplicate, using the Qiagen AllPrep DNA/RNA Micro Kit (New England Biolab) and protocols were followed. Total DNA concentrations were determined with the Qubit DNA BR Assay (ThermoFisher, Q10211).

DNA methylation clock

Methylation data was generated via the HorvathMammalMethylChip (Arneson et al., 2022) and normalized with the SeSaMe method (Zhou et al., 2018). Human methylation data were generated on the Illumina EPIC array platforms which profiles 866k cytosines. The noob normalization method was used and implemented in the R function preprocessNoob. The DNAm age was estimated using the DNAm Age Skin Final clock algorithm (Boroni et al., 2020).

MTS cell proliferation assay

Cell viability was performed with Tetrazolium MTS assay. Cells were cultured for 1 day in 96-well plates and treated with small molecules for 3 consecutive days prior to incubation with 120 μ L fresh media containing 20 μ L of CellTiter 96[®] Aqueous One Solution (Promega, G3580) for 1–4 h at 37°C in a humidified, 5% CO₂ atmosphere. The absorbance was determined at 490 nm using a BioTek Epoch 2 microplate reader. The proportion of viable cells was determined as a ratio between the observed optical density (OD) compared to control OD.

Quantification and statistical analysis

Analysis of immunofluorescence microscopy images was performed using FIJI. Typically, 20 different ROIs were imaged at 100x from each well from three experiments unless otherwise noted. Maximal projections of z-stacks were analyzed and total fluorescence intensity per cell and total nuclear area were determined.

All statistical analysis, statistical significance and n values are reported in the figure legends. Statistical analyses were performed using GraphPad Prism 9.0.0.

Data availability statement

The datasets presented in this study can be found in online repositories. The names of the repository/repositories and accession number(s) can be found below: <https://www.ncbi.nlm.nih.gov/geo/query/acc.cgi?acc=GSE231853>, GSE231853.

Ethics statement

The animal study was approved by the University of Lausanne and Canton Vaud, animal experimentation license VD3608. The study was conducted in accordance with the local legislation and institutional requirements.

Author contributions

PTP: designed the study, was involved in all experiments, data collection, analysis and interpretation, generated the mice strains, prepared the figures, prepared and analyzed RNA-seq data, and wrote the manuscript. CR: prepared the figures, prepared and analyzed RNA-seq data and review and edited the manuscript. FM: prepared and analyzed RNA-seq data, and review and edited the manuscript. GD-M: provided guidance, and review and edited the manuscript. CM: performed skin fibroblast extractions, and review and edited the manuscript. AP: generated the mice strains, and review and edited the manuscript. AH: was involved in data collection, analysis and interpretation, and review and edited the manuscript. RB: was involved in data collection, analysis and interpretation, and review and edited the manuscript. SH: was involved in data collection, analysis and interpretation, and review and edited the manuscript. AS: prepared and analyzed RNA-seq data, and review and edited the manuscript. VG: prepared and analyzed RNA-seq data, and review and edited the manuscript. AO: designed the study, was involved in all experiments, data collection, analysis and interpretation, provided guidance, and wrote, review, and edited the manuscript.

Funding

The author(s) declare financial support was received for the research, authorship, and/or publication of this article. This work was supported by the Eccellenza grants (186969) from the Swiss National Science Foundation (SNSF), the University of Lausanne, and the Canton Vaud. GD-M was supported by the EMBO postdoctoral fellowship (EMBO ALTF 444-2021 to GD-M).

Acknowledgments

We acknowledge the contributions of the Protein Analysis Facility of UNIL including Severine Lorrain and Manfredo Quadroni as well as the Agora FACS facility, including Danny Labes. AS and VG are supported by grants from the US National Institutes on Aging, VG is supported by Michael Antonov Foundation, Impetus, and MWRF.

Conflict of interest

AP and AO were employed by the company EPITERNA SA. AH and SH were employed by the company Altos Labs, Inc.

The remaining authors declare that the research was conducted in the absence of any commercial or financial

relationships that could be construed as a potential conflict of interest.

Publisher's note

All claims expressed in this article are solely those of the authors and do not necessarily represent those of their affiliated organizations, or those of the publisher, the editors and the reviewers. Any product that

may be evaluated in this article, or claim that may be made by its manufacturer, is not guaranteed or endorsed by the publisher.

Supplementary material

The Supplementary Material for this article can be found online at: <https://www.frontiersin.org/articles/10.3389/fragi.2023.1323194/full#supplementary-material>

References

- Alle, Q., Le Borgne, E., Bensadoun, P., Lemey, C., Béchir, N., Gabanou, M., et al. (2022). A single short reprogramming early in life initiates and propagates an epigenetically related mechanism improving fitness and promoting an increased healthy lifespan. *Aging Cell* 21 (11), e13714. doi:10.1111/accel.13714
- Alle, Q., Le Borgne, E., Milhavel, O., and Lemaitre, J. M. (2021). Reprogramming: emerging strategies to rejuvenate aging cells and tissues. *Int. J. Mol. Sci.* 22 (8), 3990. doi:10.3390/ijms22083990
- Arneson, A., Haghani, A., Thompson, M. J., Pellegrini, M., Kwon, S. B., Vu, H., et al. (2022). A mammalian methylation array for profiling methylation levels at conserved sequences. *Nat. Commun.* 13 (1), 783. doi:10.1038/s41467-022-28355-z
- Bar-Nur, O., Brumbaugh, J., Verheul, C., Apostolou, E., Pruteanu-Malinici, I., Walsh, R. M., et al. (2014). Small molecules facilitate rapid and synchronous iPSC generation. *Nat. Methods* 11 (11), 1170–1176. doi:10.1038/nmeth.3142
- Benevento, M., Tonge, P. D., Puri, M. C., Hussein, S. M. I., Cloonan, N., Wood, D. L., et al. (2014). Proteome adaptation in cell reprogramming proceeds via distinct transcriptional networks. *Nat. Commun.* 5 (1), 5613. doi:10.1038/ncomms6613
- Birkisdóttir, M. B., Jaarsma, D., Brandt, R. M. C., Barnhoorn, S., van Vliet, N., Imholz, S., et al. (2021). Unlike dietary restriction, rapamycin fails to extend lifespan and reduce transcription stress in progeroid DNA repair-deficient mice. *Aging Cell* 20 (2), e13302. doi:10.1111/accel.13302
- Boroni, M., Zonari, A., Reis de Oliveira, C., Alkatib, K., Ochoa Cruz, E. A., Brace, L. E., et al. (2021). Highly accurate skin-specific methylome analysis algorithm as a platform to screen and validate therapeutics for healthy aging. *Clin. Epigenetics* 12 (1), 105. doi:10.1186/s13148-020-00899-1
- Brambrink, T., Foreman, R., Welstead, G. G., Lengner, C. J., Wernig, M., Suh, H., et al. (2008). Sequential expression of pluripotency markers during direct reprogramming of mouse somatic cells. *Cell Stem Cell* 2 (2), 151–159. doi:10.1016/j.stem.2008.01.004
- Browder, K. C., Reddy, P., Yamamoto, M., Haghani, A., Guillen, I. G., Sahu, S., et al. (2022). *In vivo* partial reprogramming alters age-associated molecular changes during physiological aging in mice. *Nat. Aging* 2 (3), 243–253. doi:10.1038/s43587-022-00183-2
- Buganim, Y., Faddah, D. A., Cheng, A. W., Itskovich, E., Markoulaki, S., Ganz, K., et al. (2012). Single-cell expression analyses during cellular reprogramming reveal an early stochastic and a late hierarchic phase. *Cell* 150 (6), 1209–1222. doi:10.1016/j.cell.2012.08.023
- Carey, B. W., Markoulaki, S., Beard, C., Hanna, J., and Jaenisch, R. (2010). Single-gene transgenic mouse strains for reprogramming adult somatic cells. *Nat. Methods* 7 (1), 56–59. doi:10.1038/nmeth.1410
- Chen, J., Liu, J., Chen, Y., Yang, J., Chen, J., Liu, H., et al. (2011). Rational optimization of reprogramming culture conditions for the generation of induced pluripotent stem cells with ultra-high efficiency and fast kinetics. *Cell Res.* 21 (6), 884–894. doi:10.1038/cr.2011.51
- Chen, Y., Lüttmann, F. F., Schoger, E., Schöler, H. R., Zelarayán, L. C., Kim, K. P., et al. (2021). Reversible reprogramming of cardiomyocytes to a fetal state drives heart regeneration in mice. *Science* 373 (6562), 1537–1540. doi:10.1126/science.abg5159
- Cheng, F., Wang, C., Ji, Y., Yang, B., Shu, J., Shi, K., et al. (2022). Partial reprogramming initiates widespread targeted chromatin remodeling. *Aging Cell* 21 (4), e13577. doi:10.1111/accel.13577
- Chondronasiou, D., Gill, D., Mosteiro, L., Urduinguo, R. G., Berenguer-Llargo, A., Aguilera, M., et al. (2022). Multi-omic rejuvenation of naturally aged tissues by a single cycle of transient reprogramming. *Aging Cell* 21 (3), e13578. doi:10.1111/accel.13578
- David, L., and Polo, J. M. (2014). Phases of reprogramming. *Stem Cell Res.* 12 (3), 754–761. doi:10.1016/j.scr.2014.03.007
- de Lázaro, I., Yilmazer, A., Nam, Y., Qubisi, S., Razak, F. M. A., Degens, H., et al. (2019). Non-viral, tumor-free induction of transient cell reprogramming in mouse skeletal muscle to enhance tissue regeneration. *Mol. Ther.* 27 (1), 59–75. doi:10.1016/j.yth.2018.10.014
- de Magalhães, J. P., and Ocampo, A. (2022). Cellular reprogramming and the rise of rejuvenation biotech. *Trends Biotechnol.* 40 (6), 639–642. doi:10.1016/j.tibtech.2022.01.011
- de Waard, M. C., van der Pluijm, I., Zuiderveen Borgesius, N., Comley, L. H., Haasdijk, E. D., Rijksen, Y., et al. (2010). Age-related motor neuron degeneration in DNA repair-deficient Ercc1 mice. *Acta Neuropathol.* 120 (4), 461–475. doi:10.1007/s00401-010-0715-9
- Dollé, M. E. T., Busuttill, R. A., Garcia, A. M., Wijnhoven, S., van Druenen, E., Niedernhofer, L. J., et al. (2006). Increased genomic instability is not a prerequisite for shortened lifespan in DNA repair deficient mice. *Mutat. Research/Fundamental Mol. Mech. Mutagen.* 596 (1), 22–35. doi:10.1016/j.mrfmmm.2005.11.008
- Ebrahimi, B. (2015). Reprogramming barriers and enhancers: strategies to enhance the efficiency and kinetics of induced pluripotency. *Cell Regen.* 4, 10. doi:10.1186/s13619-015-0024-9
- Esteban, M. A., Wang, T., Qin, B., Yang, J., Qin, D., Cai, J., et al. (2010). Vitamin C enhances the generation of mouse and human induced pluripotent stem cells. *Cell Stem Cell* 6 (1), 71–79. doi:10.1016/j.stem.2009.12.001
- Gill, D., Parry, A., Santos, F., Okkenhaug, H., Todd, C. D., Hernando-Herraez, I., et al. (2022). Multi-omic rejuvenation of human cells by maturation phase transient reprogramming. *eLife* 11, e71624. doi:10.7554/eLife.71624
- Guan, J., Wang, G., Wang, J., Zhang, Z., Fu, Y., Cheng, L., et al. (2022). Chemical reprogramming of human somatic cells to pluripotent stem cells. *Nature* 605 (7909), 325–331. doi:10.1038/s41586-022-04593-5
- Hansson, J., Rafiee, M. R., Reiland, S., Polo, J. M., Gehring, J., Okawa, S., et al. (2012). Highly coordinated proteome dynamics during reprogramming of somatic cells to pluripotency. *Cell Rep.* 2 (6), 1579–1592. doi:10.1016/j.celrep.2012.10.014
- Horvath, S. (2013). DNA methylation age of human tissues and cell types. *Genome Biol.* 14 (10), R115. doi:10.1186/gb-2013-14-10-r115
- Hou, P., Li, Y., Zhang, X., Liu, C., Guan, J., Li, H., et al. (2013). Pluripotent stem cells induced from mouse somatic cells by small-molecule compounds. *Science* 341 (6146), 651–654. doi:10.1126/science.1239278
- Kanamoto, T., Hellman, U., Heldin, C. H., and Souchelnytskyi, S. (2002). Functional proteomics of transforming growth factor-beta1-stimulated Mv1Lu epithelial cells: Rad51 as a target of TGFbeta1-dependent regulation of DNA repair. *EMBO J.* 21 (5), 1219–1230. doi:10.1093/emboj/21.5.1219
- Kane, A. E., and Sinclair, D. A. (2019). Epigenetic changes during aging and their reprogramming potential. *Crit. Rev. Biochem. Mol. Biol.* 54 (1), 61–83. doi:10.1080/10409238.2019.1570075
- Kennedy, B. K., Berger, S. L., Brunet, A., Campisi, J., Cuervo, A. M., Epel, E. S., et al. (2014). Geroscience: linking aging to chronic disease. *Cell* 159 (4), 709–713. doi:10.1016/j.cell.2014.10.039
- Kim, B. G., Malek, E., Choi, S. H., Ignatz-Hoover, J. J., and Driscoll, J. J. (2021). Novel therapies emerging in oncology to target the TGF-β pathway. *J. Hematol. Oncol.* 14 (1), 55. doi:10.1186/s13045-021-01053-x
- Koche, R. P., Smith, Z. D., Adli, M., Gu, H., Ku, M., Gnirke, A., et al. (2011). Reprogramming factor expression initiates widespread targeted chromatin remodeling. *Cell Stem Cell* 8 (1), 96–105. doi:10.1016/j.stem.2010.12.001
- Kuno, A., Nishimura, K., and Takahashi, S. (2018). Time-course transcriptome analysis of human cellular reprogramming from multiple cell types reveals the drastic change occurs between the mid phase and the late phase. *BMC Genomics* 19 (1), 9. doi:10.1186/s12864-017-4389-8
- Lapasset, L., Milhavel, O., Prieur, A., Besnard, E., Babled, A., Ait-Hamou, N., et al. (2011). Rejuvenating senescent and centenarian human cells by reprogramming through the pluripotent state. *Genes Dev.* 25 (21), 2248–2253. doi:10.1101/gad.173922.111

- Lee, J. H., Kim, E. W., Croteau, D. L., and Bohr, V. A. (2020). Heterochromatin: an epigenetic point of view in aging. *Exp. Mol. Med.* 52 (9), 1466–1474. doi:10.1038/s12276-020-00497-4
- Lee, J. Y., Kim, D. K., Ko, J. J., Kim, K. P., and Park, K. S. (2016). Rad51 regulates reprogramming efficiency through DNA repair pathway. *Dev. Reprod.* 20 (2), 163–169. doi:10.12717/DR.2016.20.2.163
- Li, R., Liang, J., Ni, S., Zhou, T., Qing, X., Li, H., et al. (2010). A mesenchymal-to-epithelial transition initiates and is required for the nuclear reprogramming of mouse fibroblasts. *Cell Stem Cell* 7 (1), 51–63. doi:10.1016/j.stem.2010.04.014
- Li, W., Liu, W., Kakoki, A., Wang, R., Adebali, O., Jiang, Y., et al. (2019). Nucleotide excision repair capacity increases during differentiation of human embryonic carcinoma cells into neurons and muscle cells. *J. Biol. Chem.* 294 (15), 5914–5922. doi:10.1074/jbc.RA119.007861
- Li, W., Zhou, H., Abujarour, R., Zhu, S., Young Joo, J., Lin, T., et al. (2009). Generation of human-induced pluripotent stem cells in the absence of exogenous Sox2. *Stem Cells* 27 (12), 2992–3000. doi:10.1002/stem.240
- Liao, Y., Smyth, G. K., and Shi, W. (2013). The Subread aligner: fast, accurate and scalable read mapping by seed-and-vote. *Nucleic Acids Res.* 41 (10), e108. doi:10.1093/nar/gkt214
- Liu, L., Zhou, W., Cheng, C. T., Ren, X., Somlo, G., Fong, M. Y., et al. (2014). TGF β induces “BRCAness” and sensitivity to PARP inhibition in breast cancer by regulating DNA-repair genes. *Mol. Cancer Res.* 12 (11), 1597–1609. doi:10.1158/1541-7786.MCR-14-0201
- Liu, Q., Lopez, K., Murnane, J., Humphrey, T., and Barcellos-Hoff, M. H. (2019). Misrepair in context: TGF β regulation of DNA repair. *Front. Oncol.* 9, 799. doi:10.3389/fonc.2019.00799
- Liu, Q., Palomero, L., Moore, J., Guix, I., Espín, R., Aytés, A., et al. (2021). Loss of TGF β signaling increases alternative end-joining DNA repair that sensitizes to genotoxic therapies across cancer types. *Sci. Transl. Med.* 13 (580), eabc4465. doi:10.1126/scitranslmed.abc4465
- Liu, X., Khan, A., Li, H., Wang, S., Chen, X., and Huang, H. (2022). Ascorbic acid in epigenetic reprogramming. *Curr. Stem Cell Res. Ther.* 17 (1), 13–25. doi:10.2174/1574888X16666210714152730
- López-León, M., Outeiro, T. F., and Goya, R. G. (2017). Cell reprogramming: therapeutic potential and the promise of rejuvenation for the aging brain. *Ageing Res. Rev.* 40, 168–181. doi:10.1016/j.arr.2017.09.002
- López-Otin, C., Blasco, M. A., Partridge, L., Serrano, M., and Kroemer, G. (2013). The hallmarks of aging. *Cell* 153 (6), 1194–1217. doi:10.1016/j.cell.2013.05.039
- Lu, J. Y., Simon, M., Zhao, Y., Ablaeva, J., Corson, N., Choi, Y., et al. (2022). Comparative transcriptomics reveals circadian and pluripotency networks as two pillars of longevity regulation. *Cell Metab.* 34 (6), 836–856.e5. doi:10.1016/j.cmet.2022.04.011
- Lu, Y., Brommer, B., Tian, X., Krishnan, A., Meer, M., Wang, C., et al. (2020). Reprogramming to recover youthful epigenetic information and restore vision. *Nature* 588 (7836), 124–129. doi:10.1038/s41586-020-2975-4
- Lyu, G., Guan, Y., Zhang, C., Zong, L., Sun, L., Huang, X., et al. (2018). TGF- β signaling alters H4K20me3 status via miR-29 and contributes to cellular senescence and cardiac aging. *Nat. Commun.* 9 (1), 2560. doi:10.1038/s41467-018-04994-z
- Macip, C. C., Hasan, R., Hoznek, V., Kim, J., Metzger, L. E., Sethna, S., et al. (2023). Gene therapy mediated partial reprogramming extends lifespan and reverses age-related changes in aged mice. bioRxiv. p. 2023.01.04.522507. Available from: <https://www.biorxiv.org/content/10.1101/2023.01.04.522507v1> (Accessed January 30, 2023).
- Mah, N., Wang, Y., Liao, M. C., Prigione, A., Jozefczuk, J., Lichtner, B., et al. (2011). Molecular insights into reprogramming-initiation events mediated by the OSKM gene regulatory network. *PLOS ONE* 6 (8), e24351. doi:10.1371/journal.pone.0024351
- Maherali, N., Sridharan, R., Xie, W., Utikal, J., Eminli, S., Arnold, K., et al. (2007). Directly reprogrammed fibroblasts show global epigenetic remodeling and widespread tissue contribution. *Cell Stem Cell* 1 (1), 55–70. doi:10.1016/j.stem.2007.05.014
- Mahmoudi, S., Mancini, E., Xu, L., Moore, A., Jahanbani, F., Hebestreit, K., et al. (2019b) (2019b). Heterogeneity in old fibroblasts is linked to variability in reprogramming and wound healing. *Nature* 574 (7779), 553–558. doi:10.1038/s41586-019-1658-5
- Mahmoudi, S., Xu, L., and Brunet, A. (2019a). Turning back time with emerging rejuvenation strategies. *Nat. Cell Biol.* 21 (1), 32–43. doi:10.1038/s41556-018-0206-0
- Manukyan, M., and Singh, P. B. (2014). Epigenome rejuvenation: HP1 β mobility as a measure of pluripotent and senescent chromatin ground states. *Sci. Rep.* 4 (1), 4789. doi:10.1038/srep04789
- Mikkelsen, T. S., Hanna, J., Zhang, X., Ku, M., Wernig, M., Schorderet, P., et al. (2008). Dissecting direct reprogramming through integrative genomic analysis. *Nature* 454 (7200), 49–55. doi:10.1038/nature07056
- Niedernhofer, L. J., Gurkar, A. U., Wang, Y., Vijg, J., Hoeijmakers, J. H. J., and Robbins, P. D. (2018). Nuclear genomic instability and aging. *Annu. Rev. Biochem.* 87 (1), 295–322. doi:10.1146/annurev-biochem-062917-012239
- Ocampo, A., Reddy, P., Martinez-Redondo, P., Platero-Luengo, A., Hatanaka, F., Hishida, T., et al. (2016). *In vivo* amelioration of age-associated hallmarks by partial reprogramming. *Cell* 167 (7), 1719–1733.e12. doi:10.1016/j.cell.2016.11.052
- Olova, N., Simpson, D. J., Marioni, R. E., and Chandra, T. (2019). Partial reprogramming induces a steady decline in epigenetic age before loss of somatic identity. *Aging Cell* 18 (1), e12877. doi:10.1111/acel.12877
- Pal, D., Pertot, A., Shirole, N. H., Yao, Z., Anaparthi, N., Garvin, T., et al. (2017). TGF- β reduces DNA ds-break repair mechanisms to heighten genetic diversity and adaptability of CD44+/CD24- cancer cells. *eLife* 6, e21615. doi:10.7554/eLife.21615
- Perez, K., Parras, A., Rechsteiner, C., Haghani, A., Brooke, R., Mrabti, C., et al. (2022). ERCC1 mice, unlike other premature aging models, display accelerated epigenetic age. bioRxiv. p. 2022.12.28.522011. Available from: <https://www.biorxiv.org/content/10.1101/2022.12.28.522011v1> (Accessed April 13, 2023).
- Plath, K., and Lowry, W. E. (2011). Progress in understanding reprogramming to the induced pluripotent state. *Nat. Rev. Genet.* 12 (4), 253–265. doi:10.1038/nrg2955
- Polo, J. M., Anderssen, E., Walsh, R. M., Schwarz, B. A., Nefzger, C. M., Lim, S. M., et al. (2012). A molecular roadmap of reprogramming somatic cells into iPS cells. *Cell* 151 (7), 1617–1632. doi:10.1016/j.cell.2012.11.039
- Rando, T. A., and Chang, H. Y. (2012). Aging, rejuvenation, and epigenetic reprogramming: resetting the aging clock. *Cell* 148 (1), 46–57. doi:10.1016/j.cell.2012.01.003
- Roux, A. E., Zhang, C., Paw, J., Zavala-Solorio, J., Malahias, E., Vijay, T., et al. (2022). Diverse partial reprogramming strategies restore youthful gene expression and transiently suppress cell identity. *Cell Syst.* 13 (7), 574–587.e11. doi:10.1016/j.cels.2022.05.002
- Samavarchi-Tehrani, P., Golipour, A., David, L., Sung, H., Beyer, T. A., Datti, A., et al. (2010). Functional genomics reveals a BMP-driven mesenchymal-to-epithelial transition in the initiation of somatic cell reprogramming. *Cell Stem Cell* 7 (1), 64–77. doi:10.1016/j.stem.2010.04.015
- Sarkar, T. J., Quarta, M., Mukherjee, S., Colville, A., Paine, P., Doan, L., et al. (2020). Transient non-integrative expression of nuclear reprogramming factors promotes multifaceted amelioration of aging in human cells. *Nat. Commun.* 11 (1), 1545. doi:10.1038/s41467-020-15174-3
- Schoenfeldt, L., Paine, P. T., Kamaludeen, N. H., Phelps, G. B., Mrabti, C., Perez, K., et al. (2022). Chemical reprogramming ameliorates cellular hallmarks of aging and extends lifespan. bioRxiv. p. 2022.08.29.505222. Available from: <https://www.biorxiv.org/content/10.1101/2022.08.29.505222v1> (Accessed February 14, 2023).
- Schumacher, B., Pothof, J., Vijg, J., and Hoeijmakers, J. H. J. (2021). The central role of DNA damage in the ageing process. *Nature* 592 (7856), 695–703. doi:10.1038/s41586-021-03307-7
- Singh, P. B., and Newman, A. G. (2018). Age reprogramming and epigenetic rejuvenation. *Epigenetics Chromatin.* 11 (1), 73. doi:10.1186/s13072-018-0244-7
- Stadtfield, M., and Hochedlinger, K. (2010). Induced pluripotency: history, mechanisms, and applications. *Genes Dev.* 24 (20), 2239–2263. doi:10.1101/gad.1963910
- Stadtfield, M., Maherali, N., Borkent, M., and Hochedlinger, K. (2010). A reprogrammable mouse strain from gene-targeted embryonic stem cells. *Nat. Methods* 7 (1), 53–55. doi:10.1038/nmeth.1409
- Stadtfield, M., Maherali, N., Breault, D. T., and Hochedlinger, K. (2008). Defining molecular cornerstones during fibroblast to iPSC cell reprogramming in mouse. *Cell Stem Cell* 2 (3), 230–240. doi:10.1016/j.stem.2008.02.001
- Takahashi, K., and Yamanaka, S. (2006). Induction of pluripotent stem cells from mouse embryonic and adult fibroblast cultures by defined factors. *Cell* 126 (4), 663–676. doi:10.1016/j.cell.2006.07.024
- Takata, H., Hanafusa, T., Mori, T., Shimura, M., Iida, Y., Ishikawa, K., et al. (2013). Chromatin compaction protects genomic DNA from radiation damage. *PLoS One* 8 (10), e75622. doi:10.1371/journal.pone.0075622
- Takayama, K., Kawakami, Y., Lavasani, M., Mu, X., Cummins, J. H., Yurube, T., et al. (2017). mTOR signaling plays a critical role in the defects observed in muscle-derived stem/progenitor cells isolated from a murine model of accelerated aging. *J. Orthop. Res.* 35 (7), 1375–1382. doi:10.1002/jor.23409
- Tian, X., Firsanov, D., Zhang, Z., Cheng, Y., Luo, L., Tomblin, G., et al. (2019). SIRT6 is responsible for more efficient DNA double-strand break repair in long-lived species. *Cell* 177 (3), 622–638. doi:10.1016/j.cell.2019.03.043
- Tominaga, K., and Suzuki, H. I. (2019). TGF- β signaling in cellular senescence and aging-related pathology. *Int. J. Mol. Sci.* 20 (20), 5002. doi:10.3390/ijms20205002
- Tubbs, A., and Nussenzweig, A. (2017). Endogenous DNA damage as a source of genomic instability in cancer. *Cell* 168 (4), 644–656. doi:10.1016/j.cell.2017.01.002
- Vermeij, W. P., Dollé, M. E. T., Reiling, E., Jaarsma, D., Payan-Gomez, C., Bombardieri, C. R., et al. (2016). Restricted diet delays accelerated ageing and genomic stress in DNA-repair-deficient mice. *Nature* 537 (7620), 427–431. doi:10.1038/nature19329
- Vidal, S. E., Amlani, B., Chen, T., Tsrigras, A., and Stadtfield, M. (2014). Combinatorial modulation of signaling pathways reveals cell-type-specific requirements for highly

efficient and synchronous iPSC reprogramming. *Stem Cell Rep.* 3 (4), 574–584. doi:10.1016/j.stemcr.2014.08.003

Wang, C., Rabadan Ros, R., Martinez-Redondo, P., Ma, Z., Shi, L., Xue, Y., et al. (2021). *In vivo* partial reprogramming of myofibers promotes muscle regeneration by remodeling the stem cell niche. *Nat. Commun.* 12 (1), 3094. doi:10.1038/s41467-021-23353-z

Weeda, G., Donker, I., de Wit, J., Morreau, H., Janssens, R., Vissers, C. J., et al. (1997). Disruption of mouse ERCC1 results in a novel repair syndrome with growth failure, nuclear abnormalities and senescence. *Curr. Biol.* 7 (6), 427–439. doi:10.1016/s0960-9822(06)00190-4

Weiss, A., and Attisano, L. (2013). The TGFbeta superfamily signaling pathway. *WIREs Dev. Biol.* 2 (1), 47–63. doi:10.1002/wdev.86

Yang, J. H., Hayano, M., Griffin, P. T., Amorim, J. A., Bonkowski, M. S., Apostolides, J. K., et al. (2023). Loss of epigenetic information as a cause of mammalian aging. *Cell* 186 (2), 305–326.e27. doi:10.1016/j.cell.2022.12.027

Zhang, H., Kozono, D. E., O'Connor, K. W., Vidal-Cardenas, S., Rousseau, A., Hamilton, A., et al. (2016). TGF-B inhibition rescues hematopoietic stem cell defects and bone marrow failure in fanconi anemia. *Cell Stem Cell* 18 (5), 668–681. doi:10.1016/j.stem.2016.03.002

Zhou, W., Triche, T. J., Jr, Laird, P. W., and Shen, H. (2018). SeSAMe: reducing artifactual detection of DNA methylation by Infinium BeadChips in genomic deletions. *Nucleic Acids Res.* 46 (20), e123. doi:10.1093/nar/gky691